Diao, H., Robinson, P., Wisnom, M. R., & Bismarck, A. (2016). Unidirectional carbon fibre reinforced polyamide-12 composites with enhanced strain to tensile failure by introducing fibre waviness. *Composites Part A: Applied Science and Manufacturing*, *87*, 186-193. https://doi.org/10.1016/j.compositesa.2016.04.025

Unidirectional carbon fibre reinforced polyamide-12 composites with enhanced strain to tensile failure by introducing fibre waviness

Hele Diao[a], Paul Robinson[b], Michael R. Wisnom[c] and Alexander Bismarck[a,d,*]

[a] Polymer and Composite Engineering Group, Chemical Engineering Department, Imperial College London, Exhibition Road, London, SW7 2AZ, United Kingdom

[b] The Composite Centre, Aeronautics Department, Imperial College London, Exhibition Road, London, SW7 2AZ, United Kingdom

[c] Advanced Composite Centre for Innovation and Science, Department of Aerospace Engineering, University of Bristol, University Walk, Bristol, BS8 1TR, United Kingdom

[d] Polymer and Composite Engineering Group, Institute of Materials Chemistry and Research, University of Vienna, Währinger Str. 42, A-1090 Wien, Austria

[*] Corresponding Author: a.bismarck@imperial.ac.uk; alexander.bismarck@univie.ac.uk

Abstract

Unidirectional (UD) carbon fibre reinforced polymers offer high specific strength and stiffness but they fail in a catastrophic manner with little warning. Gas-texturing and non-constrained annealing were used to introduce fibre waviness into UD polyamide 12 composites produced by wet-impregnation hoping to produce composites with a more gradual failure mode and increased failure strain. Both methods increased the variation of fibre alignment angle compared to the control samples. The composites containing wavy fibres exhibited a stepwise, gradual failure mode under strain controlled uniaxial tension rather than a catastrophic failure, observed in control samples. Gas-texturing damaged the fibres resulting in a decrease of the tensile strength and strain to failure, which resulted in composites with lower tensile strength and ultimate failure strain than

the control composites. Non-constrained annealing of carbon fibre/PA-12 produced wavy fibre composites with ultimate failure strain of 2%, significantly higher than 1.6% of the control composite.

Keywords: A. Polymer-matrix composites (PMCs); A. Carbon fibre; B. Mechanical properties.

1 Introduction

Unidirectional (UD) carbon fibre reinforced polymers have higher specific strength and stiffness, longer fatigue life and higher corrosion resistance than metallic materials [1]. Nowadays, they are used in the aeronautic and automobile industries, wind energy, civil engineering and luxury sports goods. However, most UD carbon fibre reinforced polymers (CFRPs) fail at strains of 1.4%-1.8%[1,2,3] under uniaxial tension. Failure normally occurs in a sudden and catastrophic manner, which means that this material provides no prior warning and has no residual load carrying capacity.

In order to increase the failure strain of UD CFRPs and change the catastrophic failure mode into a more gradual one, researchers have used different techniques, for instance, thin-ply hybridisation [2-4], thin-ply CFRP angle ply lamination [5], wavy-ply sandwich structures [6] and interleaved lamination [7]. In addition to these techniques, another possibility is to combine wavy fibres with straight fibres in a polymer matrix. One of the possible failure mechanisms of such composites subjected to uniaxial tensile strain is that the straight, well-aligned fibres fail first while the wavy fibres align in the

[1] *Data sheet of HexPly 8552*, [Data sheet] 2013. Accessed on 2014 15/09; Available from: http://www.hexcel.com/Resources/DataSheets/Prepreg-Data-Sheets/8552_us.pdf
[2] *Data sheet of HexPly 913*, [Data sheet] 2014. Accessed on 2014 15/09; Available from: http://www.hexcel.com/Resources/DataSheets/Prepreg-Data-Sheets/913_eu.pdf
[3] *Data sheet of TORAYCA T700S*, 2013. Accessed on 2014 15/09; Available from: http://www.toraycfa.com/pdfs/T700SDataSheet.pdf

direction of applied strain and can sustain higher applied strains until they eventually fail. The effect of out-of-plane ply waviness on the behaviour of UD composites in compression was studied in great detail [8-15]. However, there seems to be much less known about the tensile behaviour of wavy fibre UD composites. Kuo et al. [16] and Chun et al. [12] found that the tensile failure strain of UD composites containing uniform or random out-of plane ply waviness is higher than the tensile strain of UD composite only containing straight fibre plies. Mukhopadhyay et al. [17] studied the effect of ply wrinkles on the tensile behaviour of quasi-isotropic composite laminates. They found that the out-of-plane ply wrinkle acted as a local shear stress concentrator, resulting in delamination before fibre failure. All the work stated above focused on studying the mechanical behaviour of composites containing wavy plies in the out-of-plane direction, but little work has been done to study the tensile behaviour of UD composite containing in-plane wavy fibres at the filament level. One of the difficulties is to manufacture such composites. Lauke et al. [18] observed fibre misalignment and waviness in a hybrid glass/polyamide fibre tow when using a gas-texturing and pultrusion technique to manufacture a UD glass fibre/polyamide composite. The fibre misalignment was attributed to the gas-texturing process. Some investigations showed that the coefficient of thermal expansion (CTE) mismatch between composite materials and mould tools [19] and the CTE mismatch between fibres and thermoplastic matrix [20] can cause residual thermal stress in the fibres, which are large enough to create fibre waviness in UD composites at a filament level. Kugler et al. [19] observed fibre waviness with a maximum fibre misalignment of 8.4° in a carbon fibre/PSU composite when investigating the effect of different processing parameters (mould materials, moulding temperature and time) on fibre waviness in the resulting composites.

Inspired by the possibility of tailoring the strain to tensile failure of UD composites by introducing fibre waviness, two manufacturing methods were explored for producing such composites containing wavy fibres at a filament level. These were: a) gas-texturing of a carbon fibre tow followed by wet-impregnation and b) non-constrained annealing of UD carbon fibre/PA-12 composites produced by wet-impregnation. The fibre alignment angles and tensile properties of these two composites and their control samples were characterised.

2 Materials and methods

2.1 Materials

Continuous carbon fibre tows (HexTow®IM7-12K), generously provided by Hexcel Co. (Cambridge, UK), were used as reinforcement. PA-12 (Vestosint®-2159), kindly supplied by Evonik Degussa GmbH (Weiterstadt, Germany) was used as the matrix. The PA-12 in powder form has an average particle size (d_{50}) of 10 μm. Its glass transition (T_g) and melting temperature (T_m) are 27 °C and 183 °C, respectively. Surfactant (Cremophor® A-25), kindly provided by BASF (Manchester, UK), was used to aid the (re)dispersion of the polymer powder. Nitrogen (BOC UK Co., London, UK) was used for the gas-texturing process.

2.2 Manufacturing UD CF/PA-12 composite tapes using a gas-texturing method followed by wet-powder impregnation

Gas-textured carbon fibre reinforced PA-12 tape was manufactured using a modular custom-built composite production line (CPL) [21] (developed by the Polymer and Composite Engineering Group at Imperial College London, see schematic diagram in Fig. 1).

Two litres of a PA-12/water dispersion (5 wt.%) was prepared for the wet-impregnation bath of the CPL. To aid the dispersion of the polymer powder and avoid cake formation during rest periods, 0.1 wt.% surfactant was added to the suspension. In order to ensure that the PA-12 powder was homogenously distributed in the impregnation bath, this suspension was stirred at a speed of 500 rpm for 2.5 h.

Prior to entering the impregnation bath, two carbon fibre tows were passed over a perforated PTFE bar (Fig. 2), which is not free to rotate. N_2 was forced through the small holes ($Ø_{hole}$ = 1 mm) in the bar under an overpressure of 250 kPa, which caused the carbon fibre tows to spread resulting in some fibre misalignment. These spread carbon fibre tows were combined into one carbon fibre tow after the gas-texturing process.

The tow was then passed through the wet-impregnation bath alternating under and over 13 pins to spread the tow in the bath and so improve the pick-up of PA-12 powder from the suspension. A 1 m long infrared heating oven operating at a temperature of 120 °C was used to evaporate the water carried by the fibre tow exiting the bath. The PA-12 powder was melted in a second oven operating at 205 °C. After exiting the oven, the melt impregnated fibre tow passed over and under three heated shear pins operated at 220 °C to evenly distribute the polymer melt within the tow. Finally, the tow was consolidated between two steel rollers. A two-belt puller was used to pull the tape at a constant speed of 0.5 m/min. Control carbon fibre/PA-12 composite tapes were manufactured using the same process but without passing the fibres over the gas-texturing device.

During the composite tape manufacturing process, the concentration of polymer powder in the wet-impregnation bath decreases, which results in an increasing fibre volume

fraction of the produced composite. In order to maintain the powder concentration, 50 mL of concentrated PA-12 suspension (15 wt.%) was added into the bath every 15 min. The fibre volume fraction of the composite (V_f) was monitored by periodically weighing 1 m of the produced composite tape. V_f was calculated using Eq. 1:

$$V_f = \frac{\rho_m W_f}{\rho_f (W_c - W_f) + \rho_m W_f} \quad \text{Eq. 1}$$

where ρ is the density of the materials (g/m^3); W the linear weight of the composite tape (g/m). The subscripts c, m and f represent composite, polymer matrix and fibre, respectively. V_f of the produced composite tape was controlled to vary between 58-62%. Micrographs of polished cross-sections of control and gas-textured carbon fibre/PA-12 composite tapes are shown in Fig. 3(a) and (b).

2.3 Inducing fibre waviness into carbon fibre/PA-12 using non-constrained annealing

Another way to introduce fibre waviness into carbon fibre/PA-12 is non-constrained annealing. Two factors create residual thermal stress in composites resulting in fibre waviness: a) the mismatch between the CTE of carbon fibres and PA-12 and b) slowly cooling the PA-12 melt resulting in crystallisation of the PA-12.

The manufactured carbon fibre/PA-12 tape had a width of 6-8 mm and was cut into 200 mm long sections. These tape sections were sandwiched between release films (Upilex® 25S, UBE Industries Ltd., Tokyo, Japan) and placed between two steel plates. The whole assembly was heated in a pre-heated hot press (Model# 4126, Carver Inc., Indiana, USA) with a set temperature of 220 °C with contact-only pressure (i.e. no external pressure applied) for 2 h. The press was slowly cooled down to room temperature over 8 h. After the non-constrained annealing, some visible fibre misalignment was introduced into the carbon fibre/PA-12 tape (Fig. 4).

2.4 Single-fibre tensile tests on as-received and gas-textured carbon fibres

A Linkam TST350 tensile tester (Linkam Scientific Instrument Ltd, Surrey, UK) with a 20 N load cell was used to measure the tensile strength and the apparent modulus of as-received and gas-textured carbon fibres according to standard ISO 11566. For the as-received fibres, the carbon fibre tow was fixed with adhesive tape at one end and gently shaken until the filament become loosened and spread apart at the free end. A filament to be tested was randomly picked by hand from the loosened carbon fibre tow. For the gas-textured fibre, because the carbon fibre tow was already loosened by the gas-texturing process, single filaments could be easily selected from the tow. Single fibres were glued at each end to a cardboard frame to minimise the stress concentration on the fibre in the gripping area. Special care to avoid any contact in the gauge length was taken during the sample preparation to prevent the damage of the filament. The gauge length of the specimen was 25 mm and each specimen was loaded under tension at a crosshead displacement rate of 15 μm/s. The load-crosshead displacement curve was recorded until the fibre failed. At least 25 single fibres from each group, i.e. as-received and gas-textured, were tested in order to obtain representative results. The tensile strength ($\hat{\sigma}$) and strain to failure ($\hat{\varepsilon}$) of the fibres were calculated using Eq. 2 and Eq. 3, respectively:

$$\hat{\sigma} = \frac{4F_{\max}}{\pi d^2} \qquad \text{Eq. 2}$$

$$\hat{\varepsilon} = \frac{\delta}{L} \qquad \text{Eq. 3}$$

where F_{max} is the maximum measured tensile load, d the fibre diameter[4] (the fibre used in this research has circular cross section), δ the crosshead displacement when the fibre

[4] *Data sheet of HexTow IM7*, [Data sheet] 2014. Accessed on 2014 15/09; Available from: http://www.hexcel.com/resources/datasheets/carbon-fiber-data-sheets/im7.pdf

failed and L the gauge length. The apparent tensile modulus E is the slope of the linear fit to the tensile stress-strain curve.

In order to evaluate the variation and distribution of the carbon fibre tensile strength, the cumulative failure probability $P_{R,i}$ of the ith fibre was calculated using Eq. 4. The Weibull-modulus (m) of the fibre strength is given by the slope of the plot of $\ln[-\ln(1-P_{R,i})]$ as a function of $\ln\hat{\sigma}_i$ (Eq. 5) [22],

$$P_{R,i} = \frac{R_i}{N+1} \quad \text{Eq. 4}$$

$$\ln[-\ln(1-P_{R,i})] = m\ln\hat{\sigma}_i + C \quad \text{Eq. 5}$$

where R_i is the rank of the ith fibre, N the total number of tested fibres, $\hat{\sigma}_i$ the strength of the ith fibre and C a constant.

2.5 Tensile tests of control, gas-textured and non-constrained annealed carbon fibre/PA-12 tapes

All the carbon fibre/PA-12 tapes were cut into 200 mm-long sections and end tabbed using a woven glass fibre/epoxy laminate with a thickness of 1.5 mm and a length of 50 mm. The end tabs were bonded to the tape using cyanoacrylate adhesive (CN-general, Techni Measure Co, Japan). The samples were tested under uniaxial tensile load (Model 5969, Instron Ltd, Bucks, UK) at a crosshead displacement rate of 0.5 mm/min. A video-gauge system was used to measure the strain in the tested specimens over a gauge length of 80 mm.

2.6 Measuring fibre alignment angle in carbon fibre/PA-12 composites

After tensile testing, the undamaged part of the samples, sandwiched by end tabs, were used to measure the fibre alignment angle in the composite via the Yurgartis' method [23]. The principle of this method is that a fibre with a circular cross-section is an ellipse when cutting it at an angle other than 90° or 0° to the fibre direction. By

measuring the major and minor axial dimensions of the ellipsoid, the individual fibre alignment angle can be obtained. Yurgartis also suggested the optimal angle between the cut-plane and nominal fibre direction for measuring fibre alignment angle was 5° [23].

In order to section the sample at an angle of 5° to the nominal fibre direction, the samples were first mounted into a specially-designed jig and then were gently ground down (see supplementary information). The sectioned samples (Fig. 5(a)) were embedded in a transparent epoxy resin (EpoxiCure®, Buehler Ltd., Düsseldorf, Germany) and cured at room temperature for 24 h. The samples were polished using a disc polish machine (Motopol-12, Buehler Ltd., Düsseldorf, Germany) with different grades of abrasion paper and diamond suspensions (details are given in Table 1). The polishing pressure and speed were 0.2 MPa and 150 rpm, respectively.

The sectioned surfaces of tested samples were investigated using a reflective microscope (AX10, Zeiss Ltd., Cambridge, UK) at 50x magnification. Twenty microscopy images were taken from each sample. A typical optical micrograph of a polished tape section is shown in Fig. 5(b). By measuring the major and minor axial dimensions of the cut fibre surfaces, the apparent fibre angle can be determined using Yurgartis' method (Eq. 6) [23]:

$$\theta_{apparent} = \sin^{-1}\frac{d}{l} \qquad \text{Eq. 6}$$

where $\theta_{apparent}$ is the apparent fibre alignment angle, l and d are the major and minor axial dimensions of the cut fibre surfaces, respectively.

For each image, 10 fibres were randomly selected for measurement. Two hundred fibre alignment angles were determined for each sample. All the tested samples in each group

(i.e. control, gas-textured and non-constrained annealed carbon fibre/PA-12) were characterised to obtain a representative result.

The apparent fibre alignment angle $\theta_{apparent}$ is a function of the fibre alignment angle in the composite and the sectioning angle φ_s. However, the sectioning angle φ_s cannot be determined with a high enough accuracy by measuring the angle between the section surface and nominal fibre direction. φ_s, therefore, has to be determined by statistical analysis of $\theta_{apparent}$. Fig. 6 shows the distribution of $\theta_{apparent}$ of a typical gas-textured carbon fibre/PA-12 tape. It is worth noting that only very few fibres seem to have an apparent fibre alignment angle smaller than 3°, which skews the apparent fibre alignment angle distribution. When the apparent fibre alignment angle is very small (less than 3°), the sectioned fibre segment is as a quasi-rectangle, which has a length exceeding the length of view field of the microscope. These fibre segments, therefore, were not considered in the measurement. In order to minimise the distortion caused by the limited field of view of the optical microscope, the sectioning angle is the median value (X_{centre}) of the gauss-fitting curves of the apparent alignment angle distribution instead of the average value of the measured apparent fibre alignment angles. The true fibre alignment angle (θ) is determined via Eq. 7:

$$\theta = \theta_{apparent} - \varphi_s \qquad \text{Eq. 7}$$

3 Results and discussion

3.1 Effect of gas-texturing on the tensile properties of carbon fibres

Typical tensile stress-strain plots of as-received and gas-textured carbon fibres are shown in Fig. 7. The tensile strength and strain to failure of gas-textured carbon fibres is 16 % lower than for as-received carbon fibres (Table 2). This is due to the fact that the gas flow misaligns the fibre filaments, causing an increase in -filament-filament contact

friction, which introduced flaws onto the filament surface. As expected, the tensile modulus of the carbon fibres is not significantly affected by the gas-texturing process.

The plots of tensile cumulative failure probability P_R as a function of the tensile strength σ of as-received and gas-textured carbon fibres fit well to the Weibull probability distribution (Fig. 8). The Weibull modulus of as-received carbon fibres is 22% higher than that of gas-textured carbon fibres, which means that the scatter in the strength of the as-received fibres is lower.

3.2 Fibre alignment angle in control, gas-textured and non-constrained annealed carbon fibre/PA-12 tapes

The distributions of the measured fibre alignment angles are presented in Fig. 9. The true fibre alignment angles of the control, gas-textured and non-constrained annealed carbon fibre/PA-12 tapes ranged from -2° to 2°, -3.5° to 4° and -4° to 5°, respectively. It can be seen that the fibre alignment angle distributions are approximately symmetric, centred about the 0° position, with higher magnitude of misalignment in the gas-textured and non-constrained annealed composites. In these cases, there appear to be fewer fibres with a misalignment angle of less than -3°, then there are with an angle greater than 3°. However, as noted earlier, this is due to the difficulties with the measurement technique, fibres at angles close to -5° have a major axis length which exceeds the length of the micrograph and so could not be counted. Despite this slight loss of symmetry, the fibre misalignment distributions of all these composites were fitted by a Gaussian distribution (Eq. 8):

$$f(\theta) = y_0 + \frac{A}{w\sqrt{\pi/2}} e^{\frac{-2(\theta-\theta_c)^2}{w^2}} \qquad \text{Eq. 8}$$

where θ_c is the median value of the Gaussian fitting curve, y_0 the offset value of the y axis of the Gaussian curve fit, A the area under the Gaussian curve fit and $y = y_0$ and w refer to the width of the peak in the Gaussian curves fits [24]. Table 3 summarises the parameters of the Gaussian curve fits of the fibre alignment angle distributions of the control, gas-textured, non-constrained carbon fibre/PA-12 composites. Compared to the control carbon fibre/PA-12, the widths of the Gaussian fitting curves of the distributions of fibre alignment angles in the gas-textured and the non-constrained annealed carbon fibre/PA-12 increased by 77% and 116%, respectively. This indicates that both the annealing process and gas texturing significantly increase the variation of the fibre alignment angles in carbon fibre/PA-12 composites.

In the carbon fibre/PA-12 control composite, 95% of fibres had less than ±1° misalignment from the axial tape direction. However, only 68.5 % of fibres in the gas-textured carbon fibre/PA-12 composites were within this misalignment angle range, i.e. still almost straight. The bulk of the remaining 31.5 % were misaligned up to ±3°, but some fibres were misaligned to an even greater extent. This was caused by the gas flow during the gas-texturing treatment, which affected the arrangement of carbon fibre filaments in the tow and so caused fibre misalignment. Similarly to the gas-textured carbon fibre/PA-12, the variation of fibre alignment angle in the non-constrained annealed carbon fibre/PA-12 is larger than that in the control samples, but now only 57.5% of fibres are aligned within ±1°. This indicates that non-constrained annealing can be successfully used to introduce variable fibre alignment angles into a carbon fibre/PA-12 composite. In this case, the fibre waviness is caused by a combination of a) the CTE mismatch between carbon fibre (-0.4×10^{-6} °C^{-1}) and PA-12 (140×10^{-6} °C^{-1}) and b) the shrinkage caused by the re-crystallisation of PA-12 (i.e. the low cooling

speed in the non-constrained annealing process allows more PA-12 chains to crystallise, resulting in a volume shrinkage of PA-12).

3.3 Tensile behaviour of control, gas-textured and non-constrained annealed carbon fibre/PA-12 tapes

A sudden and explosive failure was observed for the control carbon fibre/PA-12 composites. In the case of gas-textured and non-constrained annealed composites, part of composite failed first as the applied tensile strain increased, while the remaining part of the specimen still carried the load. When the tensile strain was further increased again an explosive failure mode was observed in both types of composites. The tensile stress-strain curves of the gas-textured and non-constrained annealed carbon fibre/PA-12 also showed a stepwise, gradual failure mode during displacement-controlled tensile tests instead of the usual sudden, catastrophic failure, which was observed for the control carbon fibre/PA-12 composites (Fig. 10). During the testing of the gas-textured and non-constrained annealed carbon fibre/PA-12 tapes, the sample still carried some load after the first failure occurred. The difference in failure modes is associated with the increase in fibre waviness present in the gas-textured and non-constrained annealed composites compared to the control samples. For a composite with a significant range of fibre waviness, the straight fibres will carry greater stress and so are more likely to fail first. Of the remaining fibres, those with least misalignment will fail next and so the failure proceeds more gradually in the gas-textured and non-constrained annealed carbon fibre/PA-12 with their larger variation of fibre alignment angles (section 3.2). It can be seen in Fig. 10 that there was no change in the ultimate failure strain of the gas-textured carbon fibre/PA-12 composites compared with the control samples. This is due to the reduction in tensile strength and failure strain of the fibres when subjected to the

gas-texturing process (section 3.1). However, it is promising that a higher ultimate failure strain was observed for the carbon fibre/PA-12 composites which were subjected to non-constrained annealing compared to the control composite. The higher ultimate failure strain for this composite was due to the fact that non-constrained annealing introduced significant fibre misalignment and waviness into the composite without damaging the carbon fibres. Compared with the control carbon fibre/PA-12 composite, the non-constrained annealed carbon fibre/PA-12 composite had higher ultimate failure strain and a more gradual failure mode.

The tensile strength, modulus and strain to failure of the control, gas-textured and non-constrained annealed carbon fibre/PA-12 tapes are summarised in Table 4. The initial tensile moduli of these three composites are similar, because the fibre misalignment angles in the gas-textured and non-constrained annealed carbon fibre/PA-12 composites are mainly within the range of -3.5° to 4° and -4° to 5° (discussed in section 3.2), which are too small to significantly affect the tensile modulus of the composite according to classic laminate theory [25]. The differences of tensile moduli of these three composites are within the standard deviation. The tensile strength of gas-textured carbon fibre/PA-12 tape is slightly smaller than that of the control composite, because the carbon fibres were damaged during gas-texturing. There was no significant change in the tensile strength of the composites after non-constrained annealing. In this case, there was no filament damage introduced by the processing technique and this therefore indicates that limited distribution of fibre misalignment achieved did not significantly affect the tensile strength.

Compressive strength of the carbon fibre/PA12 composites was investigated in the present study. However, it can be expected that fibre waviness does have a detrimental

effect on compression strength. However, where variations in angle occur over very short distances, modelling has shown that it is the average misalignment angle that controls failure [26]. Local variations in the fibre misalignment angle without a systematic overall misalignment as in this study may therefore not have a large effect on compressive strength. This requires further investigation.

4 Conclusion

Two manufacturing methods, gas-texturing and non-constrained annealing, were used to introduce fibre waviness with small fibre misalignment angles into continuous UD carbon fibre reinforced PA-12. It was found that these two manufacturing methods did increase the width of the Gaussian distribution of the fibre misalignment angle, i.e. more fibres are misaligned in these two composite compared to the control sample. In order to evaluate the effect of variations of fibre misalignment on the tensile behaviour of carbon fibre/PA-12, uniaxial tensile tests were carried out on these two composites and a control composite. Both the gas-textured and the non-constrained annealed carbon fibre/PA-12 exhibited a stepwise and more gradual tensile failure mode under displacement control in comparison to the control composite, which exhibited a sudden and catastrophic failure. However, the tensile strength of the gas-textured carbon fibre/PA-12 composite decreased and so no increase in its ultimate tensile failure strain was observed. The decrease in the tensile strength of the composite is due to the fact that the gas-texturing process damaged the carbon fibres. However, for the carbon fibre/PA-12 composites subjected to non-constrained annealing, the ultimate tensile failure strain increased without significantly affecting the tensile strength and modulus of the composite. The more gradual tensile failure mode of carbon fibre/PA-12 and the

increase in the ultimate tensile failure strain are attributed to the increase in the fibre misalignment and fibre waviness achieved in the non-constrained annealed carbon fibre/PA-12 composites in comparison to the control composite.

Acknowledgement

This work was partially funded by the UK Engineering and Physical Sciences Research Council (EPSRC) Programme Grant EP/I02946X/1 on High Performance Ductile Composite Technology (HiperDuCT). The authors are grateful for the useful discussions with Dr. John Hodgkinson (PaCE Group, Department of Chemical Engineering, Imperial College London).

References

[1] Matthews FL, Rawlings RD. Composite Materials: Engineering and Science. Cambridge: Woodhead Publishing Ltd.; 2002.
[2] Czél G, Wisnom MR. Demonstration of pseudo-ductility in high performance glass/epoxy composites by hybridisation with thin-ply carbon prepreg. Composites Part A: Applied Science and Manufacturing. 2013;52(0):23-30.
[3] Jalalvand M, Czél G, Wisnom MR. Numerical modelling of the damage modes in UD thin carbon/glass hybrid laminates. Composites Science and Technology. 2014;94(0):39-47.
[4] Czél G, Jalalvand M, Wisnom M. Design and characterisation of advanced pseudo-ductile unidirectional thin-ply carbon/epoxy– glass/epoxy hybrid composites. Composite Structures (Resubmitted after revision).
[5] Fuller JD, Wisnom MR. Pseudo-ductility and damage suppression in thin ply CFRP angle-ply laminates. Composites Part A: Applied Science and Manufacturing. 2015;69(0):64-71.
[6] Pimenta S, Robinson P. Wavy-ply sandwich with composite skins and crushable core for ductility and energy absorption. Composite Structures. 2014;116(0):364-76.
[7] Grail G, Pimenta S, Pinho ST, Robinson P. Exploring the potential of interleaving to delay catastrophic failure in unidirectional composites under tensile loading. Composites Science and Technology. 2015;106(0):100-9.
[8] Chan WS, Wang JS. Influence of fiber waviness on the structural response of composite laminates. Journal of Thermoplastic Composite Materials. 1994;7(3):243-60.
[9] Piggott MR. The effect of fibre waviness on the mechanical properties of unidirectional fibre composites: A review. Composites Science and Technology. 1995;53(2):201-5.
[10] Hsiao HM, Daniel IM. Effect of fiber waviness on stiffness and strength reduction of unidirectional composites under compressive loading. Composites Science and Technology. 1996;56(5):581-93.

[11] Wisnom MR, Atkinson JW. Fibre waviness generation and measurement and its effect on compressive strength. Journal of Reinforced Plastics and Composites. 2000;19(2):96-110.
[12] Chun H-J, Shin J-Y, Daniel IM. Effects of material and geometric nonlinearities on the tensile and compressive behavior of composite materials with fiber waviness. Composites Science and Technology. 2001;61(1):125-34.
[13] Liu D, Fleck NA, Sutcliffe MPF. Compressive strength of fibre composites with random fibre waviness. Journal of the Mechanics and Physics of Solids. 2004;52(7):1481-505.
[14] Wang J, Potter KD, Hazra K, Wisnom MR. Experimental fabrication and characterization of out-of-plane fiber waviness in continuous fiber-reinforced composites. Journal of Composite Materials. 2012;46(17):2041-53.
[15] Wang J, Potter KD, Wisnom MR, Hazra K. Failure mechanisms under compression loading in composites with designed out-of-plane fibre waviness. Plastics, Rubber and Composites. 2013;42(6):231-8.
[16] Kuo C-M, Kiyohisa T, Chou T-W. Effect of fiber waviness on the nonlinear elastic behavior of flexible composites. Journal of Composite Materials. 1988;22(11):1004-25.
[17] Mukhopadhyay S, Jones MI, Hallett SR. Tensile failure of laminates containing an embedded wrinkle; numerical and experimental study. Composites Part A: Applied Science and Manufacturing. 2015;77:219-28.
[18] Lauke B, Bunzel U, Schneider K. Effect of hybrid yarn structure on the delamination behaviour of thermoplastic composites. Composites Part A: Applied Science and Manufacturing.29A:1397-409.
[19] Kugler D, Moon TJ. Identification of the most significant processing parameters on the development of fiber waviness in thin laminates. Journal of Composite Materials. 2002;36(12):1451-79.
[20] Nairn JA. Thermoelastic analysis of residual stresses in unidirectional, high-performance composites. Polymer Composites. 1985;6(2):123-30.
[21] Ho KKC, Shamsuddin SR, Riaz S, Lamorinere S, Tran MQ, Javaid A, et al. Wet impregnation as route to unidirectional carbon fibre reinforced thermoplastic composites manufacturing. Plastics, Rubber and Composites. 2011;40(2):100-7.
[22] Bunsell AR. Handbook of Tensile Properties of Textile and Technical Fibres. Cambridge: Woodhead Publishing Limited; 2009.
[23] Yurgartis SW. Measurement of small angle fiber misalignments in continuous fibre composites. Composites Science and Technology. 1987;30:279-93.
[24] Woods J, Stark H. Probability, Statistics, and Random Processes for Engineers. Fourth Edition ed: Pearson Education; 2011.
[25] Jones RM. Mechanics of Composite Materials. London: Taylor & Francis 1999.
[26] Wisnom MR. Analysis of shear instability in compression due to fibre waviness. Journal of Reinforced Plastics and Composites. 1993;12(11):1171-89.

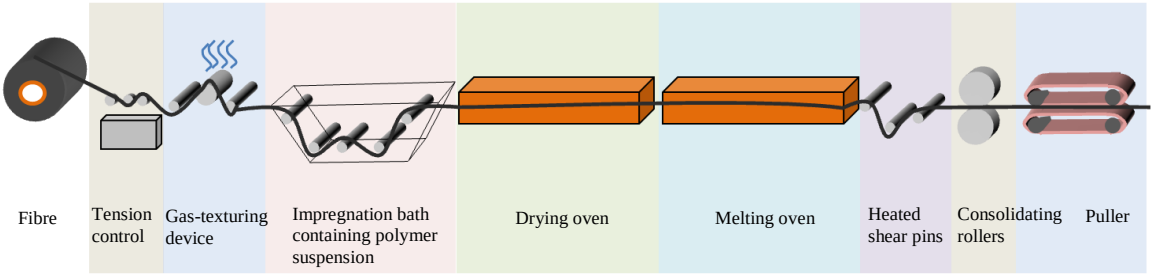

Fig. 1. Schematic diagram of setup of manufacturing route of UD carbon fibre/PA-12 composite tape

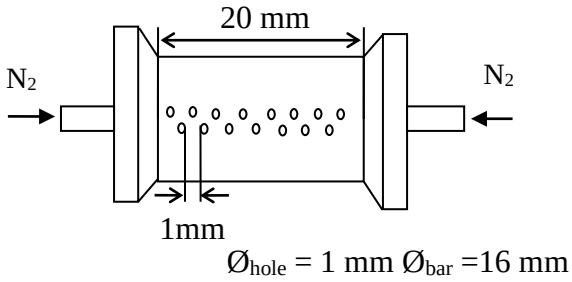

Fig. 2. Schematic drawing of the used device for gas-texturing

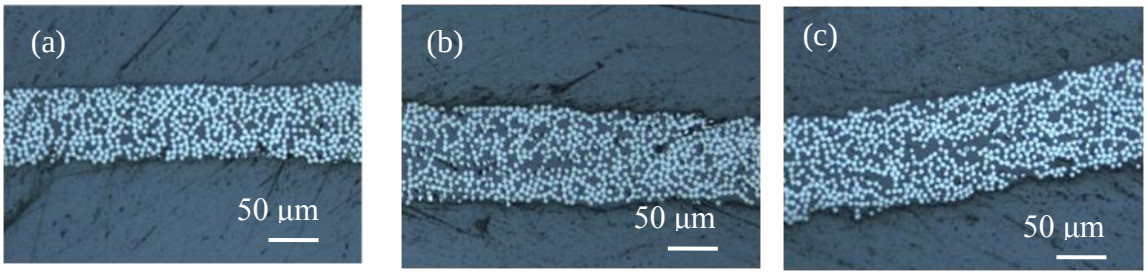

Fig. 3. Micrographs of cross section of (a) control (b) gas-textured and (c) non-constrained annealed CF/PA-12 composites

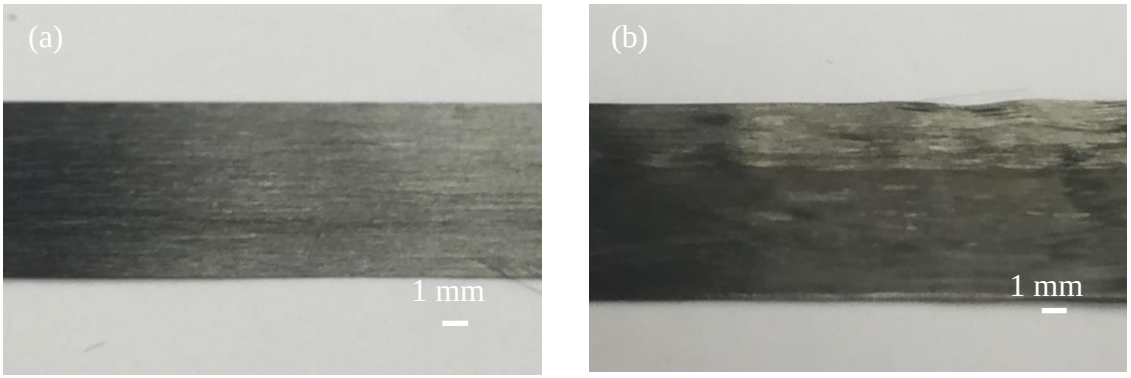

Fig. 4. Top view of the carbon fibre/PA-12 tape (a) before and (b) after non-constrained annealing

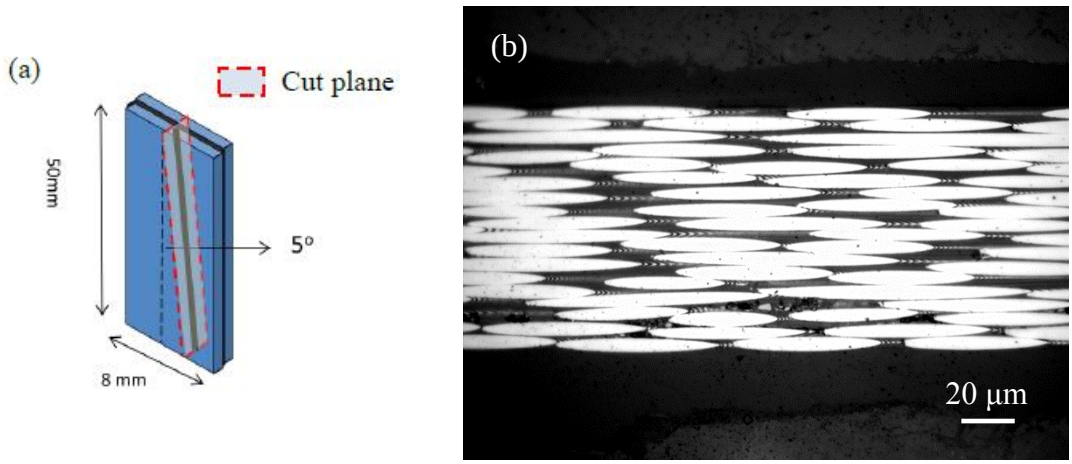

Fig. 5. (a) Schematic diagram of cutting sample (b) Typical microscope image of a polished PA12/carbon fibre composite surface

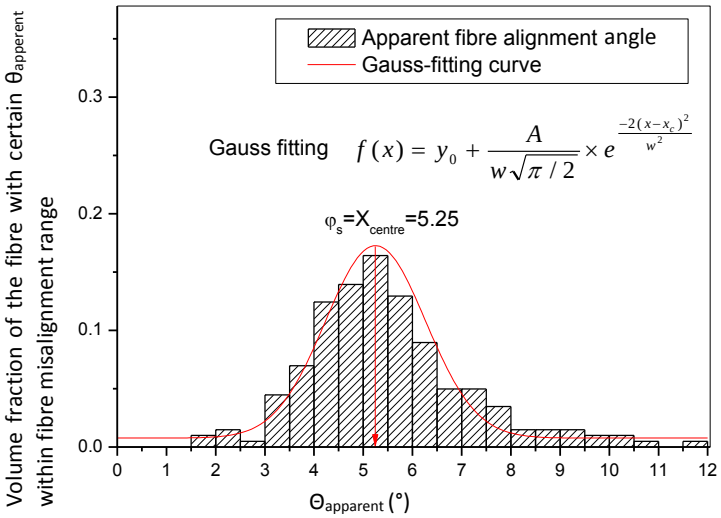

Fig. 6. Distribution of the apparent fibre alignment angles of a typical gas-textured carbon fibre/PA-12 composite

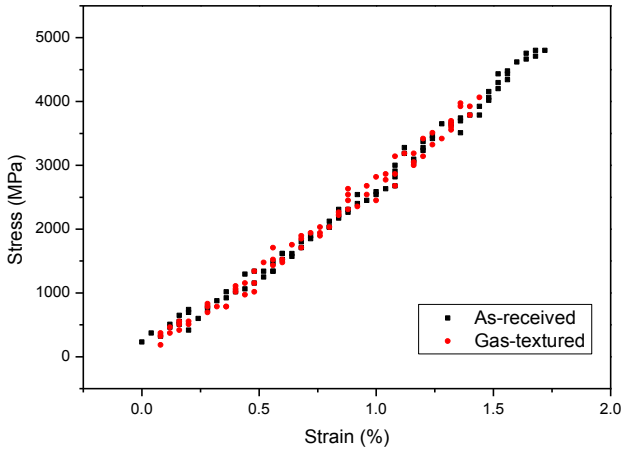

Fig. 7. Typical tensile stress-strain plots of as-received and gas-textured carbon fibres

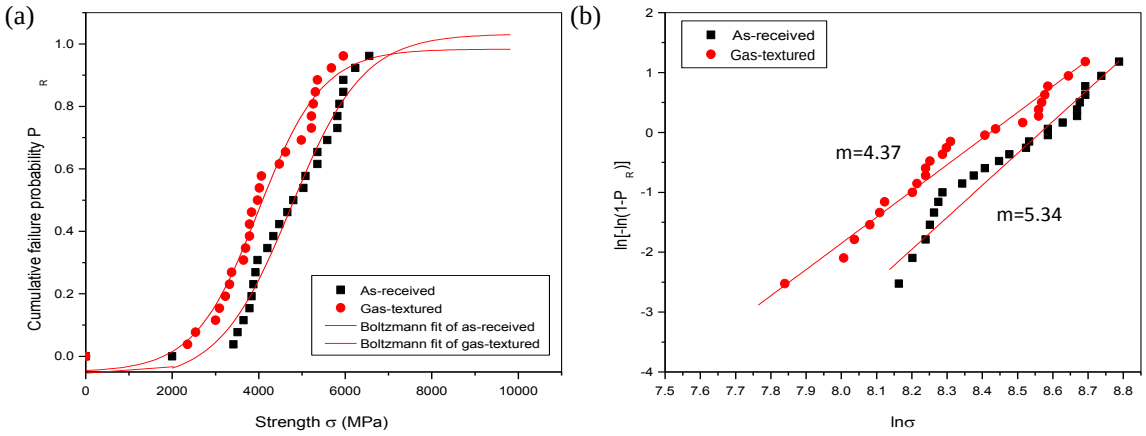

Fig. 8. (a) The cumulative failure curve and (b) Weibull plots of as-received and gas-textured carbon fibres

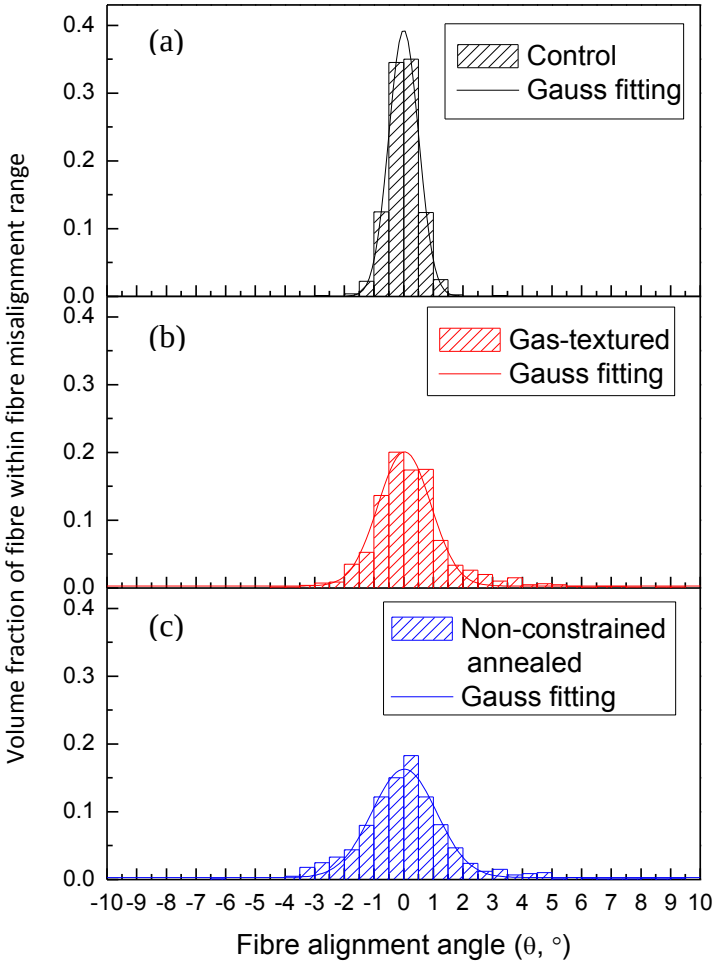

Fig. 9. True fibre alignment angle distributions of (a) control (b) gas-textured and (c) non-constrained annealed carbon fibre/PA-12 composites

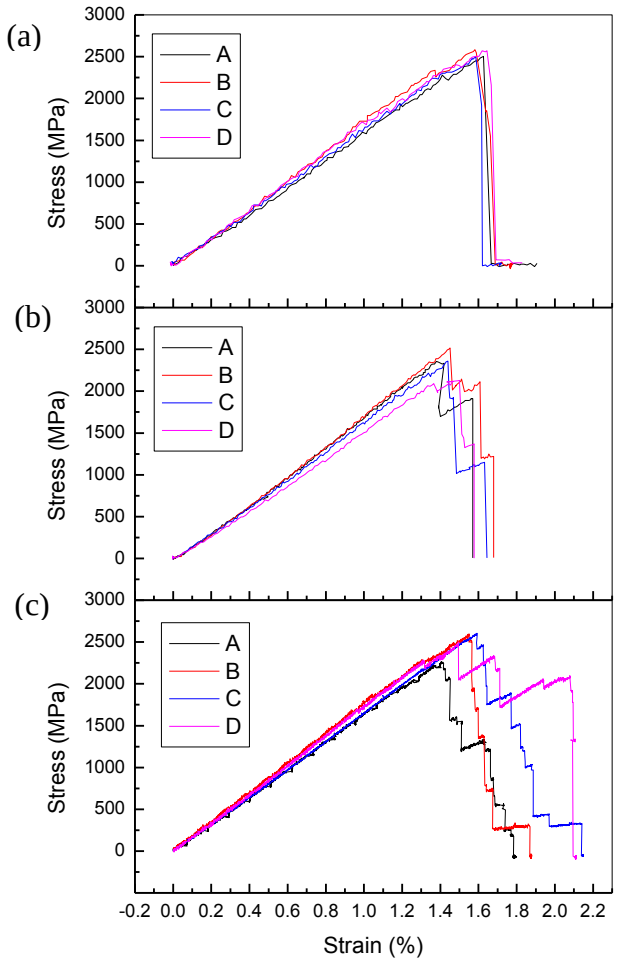

Fig. 10. Tensile stress-strain curves of (a) control, (b) gas-textured and (c) non-constrained annealed carbon fibre/PA-12 tapes

Table 1 Operation parameters of polishing process

Polishing sequence	Polishing grade	Time (min)
1	P120 SiC (with water as medium)	10
2	P320 SiC (with water as medium)	5
3	P800 SiC (with water as medium)	5
4	P2500 SiC (with water as medium)	5
5	Nylon cloth (with 6 μm diamond suspension as medium)	2
6	Nylon cloth (with 3 μm diamond suspension as medium)	2
7	Nylon cloth (with 1 μm diamond suspension as medium)	2

Table 2 Tensile properties of as-received and gas-textured carbon fibre

	Strength (MPa)	Strain to failure (%)	Modulus (GPa)	Weibull modulus of strength
As-received	4840±190	1.72±0.07	274±3	5.34
Gas-textured	4150±200	1.48±0.08	267±4	4.37

Note: "± value" is "± standard deviation"

Table 3 Parameters of the Gaussian curve fits of the distribution of the fibre alignment angles in control, gas-textured, non-constrained annealed carbon fibre/PA-12 composite

	θ_c (°)	w (°)
Control	0.00	1.00
Gas-textured	0.03	1.77
Non-constrained annealed	0.02	2.16

Table 4 Tensile properties of control, gas-textured and non-constrained annealed carbon fibre/PA-12 composite tapes

	Modulus (GPa)	Strength (MPa)	Failure strain (%)	
			Initial	Ultimate
Control	166±10	2500±100	1.61±0.03	
Gas-textured	165±7	2310±120	1.37±0.07	1.58±0.09
Non-constrained annealed	170±7	2490±160	1.51±0.08	1.96±0.16

Note: "± value" is "± standard deviation"

Supplementary

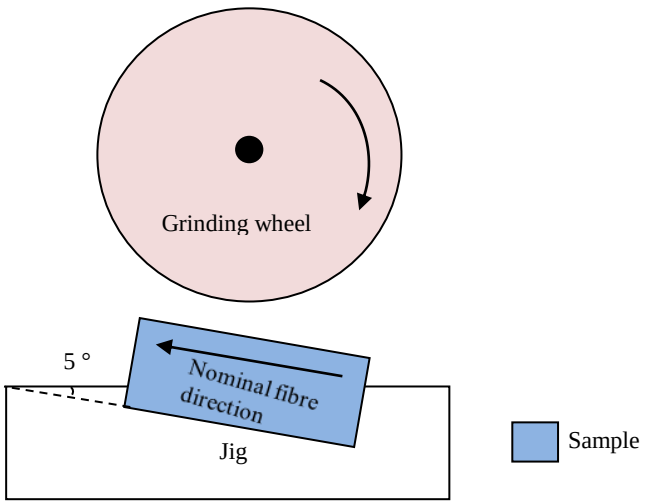

Figure (a) Schematic diagram of sectioning sample for fibre alignment angle measurement